PHILOSOPHICAL TRANSACTIONS OF THE ROYAL SOCIETY A MATHEMATICAL, PHYSICAL & ENGINEERING SCIENCES

Quasi–static deformation of particulate media

C. Thornton and S. J. Antony

Phil. Trans. R. Soc. Lond. A 1998 **356**, 2763-2782
doi: 10.1098/rsta.1998.0296

THE ROYAL SOCIETY

Quasi-static deformation of particulate media

By C. Thornton and S. J. Antony

Civil and Mechanical Engineering Division, School of Engineering and Applied Sciences, Aston University, Birmingham B4 7ET, UK

Quasi-static shear deformation of granular media is examined by performing numerical simulations on polydisperse systems of elastic spheres in a periodic cell. Results of axisymmetric compression test simulations are reported for both a dense and a loose system of spheres sheared under constant mean stress conditions. At the macroscopic scale, the simulated stress–strain-dilation responses are in excellent qualitative agreement with the mechanical behaviour of sand observed in real experiments. Numerical simulation permits a detailed examination of the evolution of internal variables associated with the micromechanical processes occurring at the particle scale. In this context, we present and discuss the evolution of the induced structural anisotropy, the percentage of sliding contacts, the average coordination number and the normal and tangential contact-force contributions to the stress tensor. Encouraged by recent research published by physicists working on granular media, we show how the distribution of normal contact forces evolves during shear, and how it is affected by changing the particle modulus and stress level. This work has led us to consider two types of interparticle contacts: (1) the contacts carrying below-average normal contact forces; and (2) the contacts carrying above-average normal contact forces. We examine how these two different categories contribute to the stress tensor and the structural anisotropy tensor. As a consequence, we present information that provides new insights into the physics of granular media and clarifies some previous findings.

Keywords: numerical simulation; granular media; quasi-static deformation; axisymmetric compression; microstructure evolution; force transmission

1. Introduction

Sands, grains and powders are granular materials whose macroscopic behaviour during quasi-static deformation is related, in some way, to the spatial and size distributions of the constituent particles and the load-displacement behaviour at the interparticle contacts. Traditional theoretical and experimental investigations of the mechanical behaviour of granular materials are restricted by the limited quantitative information about what actually happens internally. Laboratory experiments on real materials rely on estimates of the macroscopic stress and strain states from boundary measurements, which themselves depend on assumptions made about the material behaviour. Information about the internal mechanics is rare, since attempts at direct observation and measurement intrude upon the material response. In addition, comparisons between sets of test data are uncertain due to the inability to prepare exact replicas of the physical system. Traditional attempts to mathematically model the mechanical behaviour of granular media are normally based on intuitive speculation as to how the observed experimental behaviour might best be modelled by modifying existing continuum mechanics theories. However, the resulting theories invariably

include new parameters, the precise physical meaning of which is relatively obscure. This leads to difficulties in selecting appropriate experiments to rigorously test a theory.

An alternative approach is to perform computer-simulated experiments, which provide a common environment for both theory and experiment in which material properties may be precisely described and all resultant observations are quantifiable. This environment offers perfect control over experiments, non-intrusive measurements, and, with computer graphics, permits visualization of the internal micromechanical processes. The technique is well suited to the examination of assumptions and predictions of mathematical models for discrete systems, such as granular media, and is able to provide additional information not readily accessible in real physical experiments. A well-established computational technique that we have used at Aston since 1980 was developed by Cundall & Strack (1979) and is commonly known as the discrete (or distinct) element method. The method models the interactions between contiguous particles as a dynamic process and the time-evolution of the system of particles is advanced using a simple explicit finite-difference scheme.

Application of the simulation code involves cyclic calculations. At any time t, interparticle force increments are calculated at all contacts from the relative velocities of the contacting particles using incremental force-displacement rules. The interparticle forces are updated and, from the new out-of-balance force and moment on each particle, new particle accelerations (both linear and rotational) are obtained using Newton's second law. Numerical integration of the accelerations, using a small time-step, Δt, provides new particle velocities that are then numerically integrated to give displacement increments, from which the new particle positions are obtained. Having obtained new positions and velocities for all the particles, the program repeats the cycle of updating contact forces and particle locations. Checks are incorporated to identify new contacts and contacts that no longer exist. For further information about the numerical methodology, the reader is referred to Cundall & Strack (1979), Barnes (1985) and Cundall (1988).

In the original two-dimensional simulation code BALL, linear springs and dashpots were used to model the interactions between contiguous particles (Cundall & Strack 1979, 1983; Thornton & Barnes 1986), and, to simulate quasi-static deformation, it was necessary to incorporate (global) damping terms into the equations of motion in order to dissipate sufficient energy. In the Aston version of the three-dimensional simulation code TRUBAL, the interactions between contiguous spheres are modelled by algorithms based on theoretical contact mechanics. Details of the contact mechanics theories used are provided by Thornton & Yin (1991) and Thornton (1997*a*). Global damping is no longer used in the TRUBAL code. Instead, the particle density is scaled up by a factor of 10^{12} in order to provide sufficient inertial damping to permit quasi-static simulations to be performed within a reasonable time-scale.

Simulations are performed using a representative volume element, with periodic boundaries, subjected to uniform strain fields. In this way, 'perfect' experiments are created free from boundary effects. In order to control the deformation of the periodic cell, a strain-rate tensor $\dot{\varepsilon}_{ij}$ is specified, according to which the centres of all the spheres in the cell move, as though they are points in a continuum, to satisfy the equation

$$\Delta x_i = \dot{\varepsilon}_{ij} x_j \Delta t. \tag{1.1}$$

As previously described, additional incremental displacements occur as a result of the interactions between contiguous spheres. In order to follow stress-controlled loading paths, it is necessary to develop servo-control algorithms which adjust the imposed strain-rate tensor to minimize the difference between the desired and measured values of the stress tensor. The servo-control algorithms take the general form

$$\dot{\varepsilon} = \dot{\varepsilon} + g(\sigma^* - \sigma), \tag{1.2}$$

where σ^* is the desired value of stress, σ is the calculated value, and g is a gain parameter whose appropriate value is obtained by trial and error. Equation (1.2) may be expressed in terms of individual components or combinations of components of the strain-rate and stress tensors, depending on the desired loading path to be followed. More than one servo-control algorithm may be used, but care must be taken to avoid conflicting adjustments to the strain-rate tensor.

The ensemble average stress tensor is calculated from

$$\sigma_{ij} = \frac{2}{V}\sum_{1}^{M} RNn_i n_j + \frac{2}{V}\sum_{1}^{M} RTn_i t_j, \quad \text{where } n_i t_i = 0, \tag{1.3}$$

and the summations are over the M contacts in the volume V, Rn_i defines the radius vector to the contact, Nn_i and Tt_i are the normal and tangential contact forces for the contact orientation defined by the unit normal vector to the contact plane n, and t is the unit vector parallel to the contact plane.

Computer simulations of general three-dimensional quasi-static shear deformations have been performed over the complete range of deviatoric radial loading paths from axisymmetric compression to axisymmetric extension, for both dense and loose polydisperse systems of 3620 elastic spheres (Thornton & Sun 1994). The spheres had an average diameter of 0.26 mm and were given the following properties: Young's modulus, $E = 70$ GPa; Poisson's ratio, $\nu = 0.3$; coefficient of interparticle friction, $\mu = 0.3$; and interface energy, $\Gamma = 0.6\,\mathrm{J\,m^{-2}}$. Further details about the sample preparation procedures are provided by Thornton & Sun (1993, 1994). In this paper we consider only axisymmetric compression tests.

2. Macroscopic behaviour

Figure 1 shows the evolution of the deviator stress $(\sigma_1 - \sigma_3)$ with deviator strain $(\varepsilon_1 - \varepsilon_3)$ for both the dense and loose systems during axisymmetric compression, simulated with the mean stress $\frac{1}{3}(\sigma_1 + \sigma_2 + \sigma_3)$ maintained constant at 100 kPa. Figure 2 shows the corresponding evolution of the void ratio during the two simulated experiments. The two figures show that, qualitatively, the stress–strain-dilation response obtained for both the dense and loose systems is typical of that obtained in laboratory experiments. The initial shear modulus is much higher for the dense system, which exhibits a peak in the stress–strain curve at about 5% strain followed by strain-softening behaviour. The loose system does not exhibit any strain softening, the deviator stress increases at a decreasing rate until an essentially constant value is reached at about 15% strain. The volumetric strain responses, indicated by the changes in void ratio, show that the dense system expands and that the loose system contracts. At large strains, both systems deform at constant volume and this is associated with a constant deviator stress which is independent of the initial

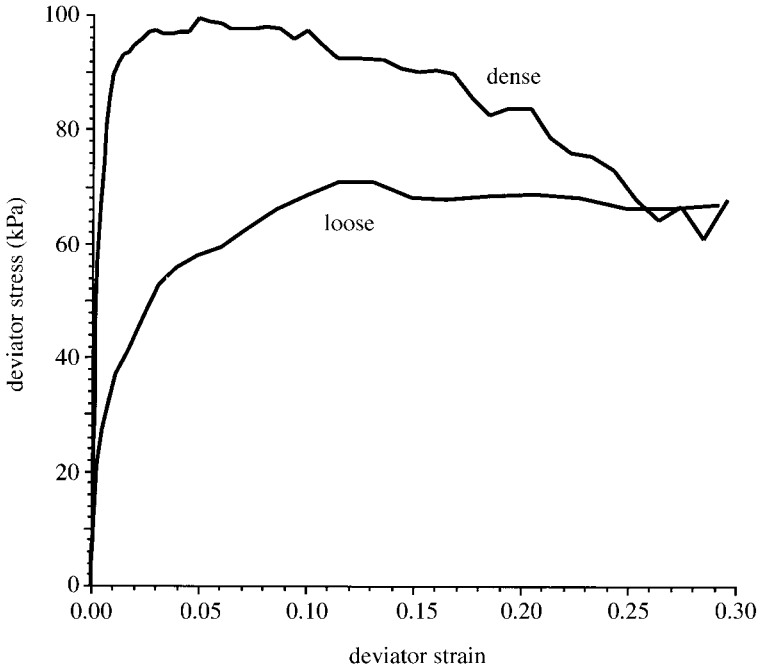

Figure 1. Evolution of deviator stress.

packing density. From traditional soil mechanics, we would expect the constant volume deformation at large strains to be associated with a 'critical void ratio' that is independent of the initial packing density. The figure shows that, at 30% deviator strain, the void ratio is not exactly the same for the two systems: 0.598 for the dense system; 0.606 for the loose system. However, in recently completed simulations on polydisperse systems of 8000 spheres, it has been found that the critical void ratio is attained at approximately 50% axial strain. In addition to the macroscopic behaviour depicted in figures 1 and 2, it is also possible, in numerically simulated experiments, to examine various internal variables and their evolution, as illustrated in § 3.

3. Evolution of internal variables

It is now well established that shear deformation of granular media produces an induced structural anisotropy that is developed primarily as a result of contact separation occurring in directions that are approximately orthogonal to the direction of the major principal stress. Structural anisotropy is defined by the distribution of contact orientations that may be represented by a probability density function, $E(\boldsymbol{n})$, and characterized by a 'fabric' tensor, ϕ_{ij} (Satake 1982), where

$$\phi_{ij} = \langle n_i n_j \rangle = \frac{1}{M} \sum_{1}^{M} n_i n_j = \frac{1}{4\pi} \int_{\Omega} E(\boldsymbol{n}) n_i n_j \, \mathrm{d}\Omega, \tag{3.1}$$

which satisfies the conditions

$$\int_{\Omega} E(\boldsymbol{n}) \, \mathrm{d}\Omega = 1 \quad \text{and} \quad E(\boldsymbol{n}) = E(-\boldsymbol{n}). \tag{3.2}$$

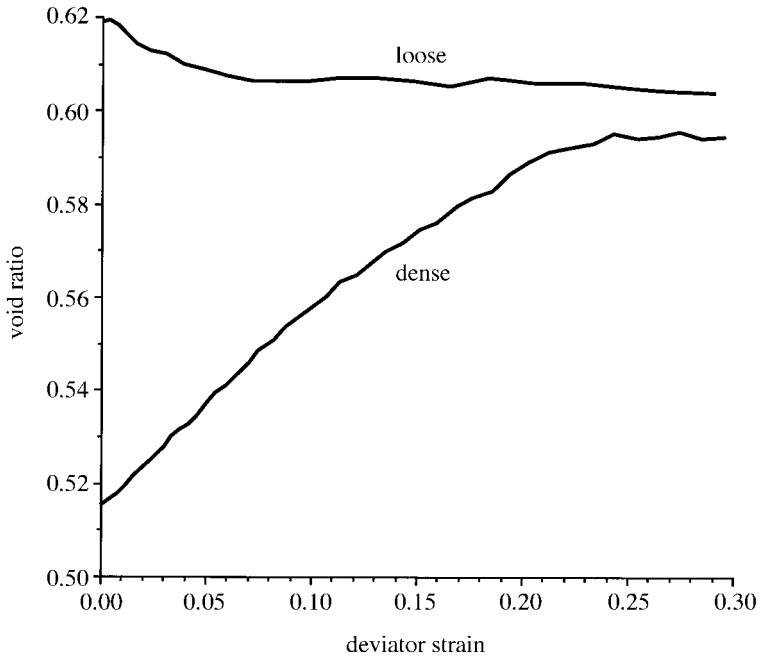

Figure 2. Evolution of void ratio.

The probability density function may be represented by a Fourier series expansion expressed in terms of even rank tensors

$$E(\boldsymbol{n}) = E_0 + E_{ij} f_{ij} + \cdots, \quad \text{where } f_{ij} = n_i n_j - \tfrac{1}{3}\delta_{ij}, \tag{3.3}$$

and

$$E_0 = \frac{1}{4\pi} \int_\Omega E(\boldsymbol{n})\, \mathrm{d}\Omega = \frac{1}{4\pi}, \tag{3.4}$$

$$E_{ij} = \frac{15}{8\pi} \int_\Omega E(\boldsymbol{n}) f_{ij}\, \mathrm{d}\Omega = \frac{15}{8\pi}(\phi_{ij} - \tfrac{1}{3}\delta_{ij}). \tag{3.5}$$

During the numerical simulations, it was confirmed that, when subjected to axisymmetric compression, the conditions $\sigma_2 = \sigma_3$ and $\phi_2 = \phi_3$ were reasonably satisfied. Consequently, the degree of induced structural anisotropy can simply be defined by the difference between the major and minor principal components of ϕ_{ij}. Figure 3 illustrates the evolution of the induced structural anisotropy, defined by the deviator fabric $(\phi_1 - \phi_3)$, for both dense and loose systems. The figure shows that the structural anisotropy increases at a decreasing rate to a maximum value that is dependent on the initial packing density. The dense system exhibits a decrease in structural anisotropy at strains in excess of 10% until, at large strains, the degree of structural anisotropy is the same for both systems. However, it can be shown that, since $E(\boldsymbol{n}) \geqslant 0$ for all orientations, the maximum possible degree of structural anisotropy under axisymmetric compression conditions is $(\phi_1 - \phi_3) = 0.25$, which is much greater than the maximum degree of anisotropy developed in the dense system. This may be attributed to the nature of the force transmission through particle systems, which will be discussed later in the paper.

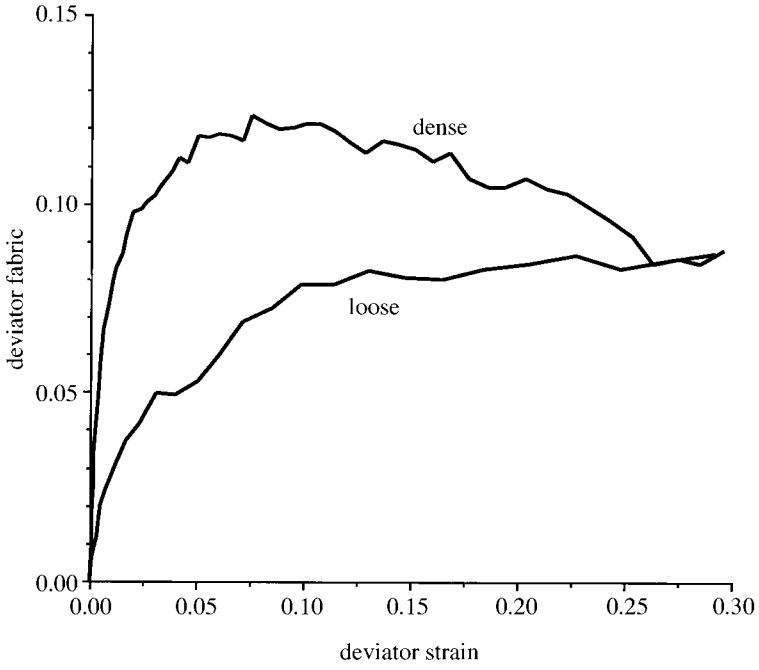

Figure 3. Evolution of induced structural anisotropy.

Equation (1.3) may be rewritten as

$$\sigma_{ij} = \sigma_{kk}\left[\frac{\langle RNn_in_j\rangle}{\langle RN\rangle} + \frac{\langle RTn_it_j\rangle}{\langle RN\rangle}\right] = \sigma_{ij}^{\mathrm{N}} + \sigma_{ij}^{\mathrm{T}}, \tag{3.6}$$

where σ_{ij}^{N} and σ_{ij}^{T} are the normal and tangential contact-force contributions to the stress tensor, respectively, and

$$\sigma_{kk} = \frac{2M}{V}\langle RN\rangle. \tag{3.7}$$

Using (3.6) to calculate the normal and tangential contact-force contributions to the stress tensor, we may examine how the normal and tangential contact forces contribute to the evolution of the deviator stress during axisymmetric compression of the dense system. The results are shown in figure 4. It can be seen that the normal contact-force contribution is the dominant contribution to the deviator stress. The tangential contact-force contribution is very small. In earlier three-dimensional simulations reported by Thornton & Sun (1993), the same phenomena were observed during axisymmetric compression of loose systems of spheres.

The average coordination number is usually defined as $Z = 2M/N$, where M is the number of contacts and N is the number of particles. However, numerical simulations have revealed that, at any time during shear, there are some particles with no contacts and some particles with only one contact. None of these particles is contributing to the stable state of stress. Hence, we define a mechanical average coordination number:

$$Z_{\mathrm{m}} = \frac{2M - N_1}{N - N_0 - N_1}, \tag{3.8}$$

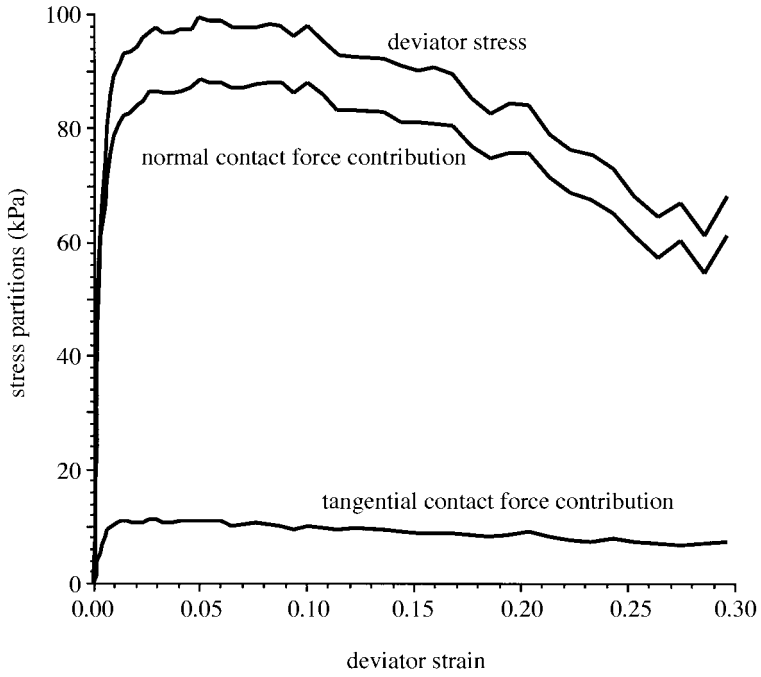

Figure 4. Evolution of normal and tangential contact-force contributions to the deviator stress (dense system).

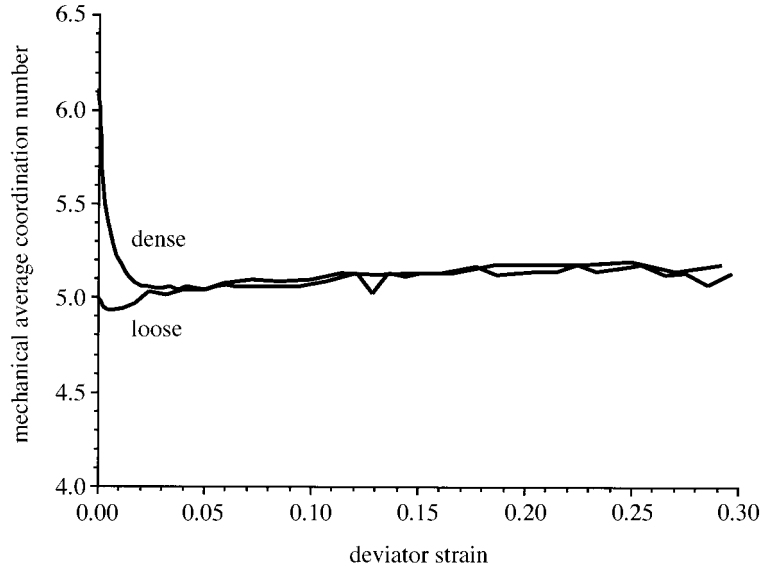

Figure 5. Evolution of the mechanical average coordination number.

where N_1 and N_0 are the number of particles with only one or no contacts, respectively.

The evolution of the mechanical average coordination number, Z_{m}, defined by (3.8) is shown in figure 5. During the initial 3% deviator strain, there is a rapid change in

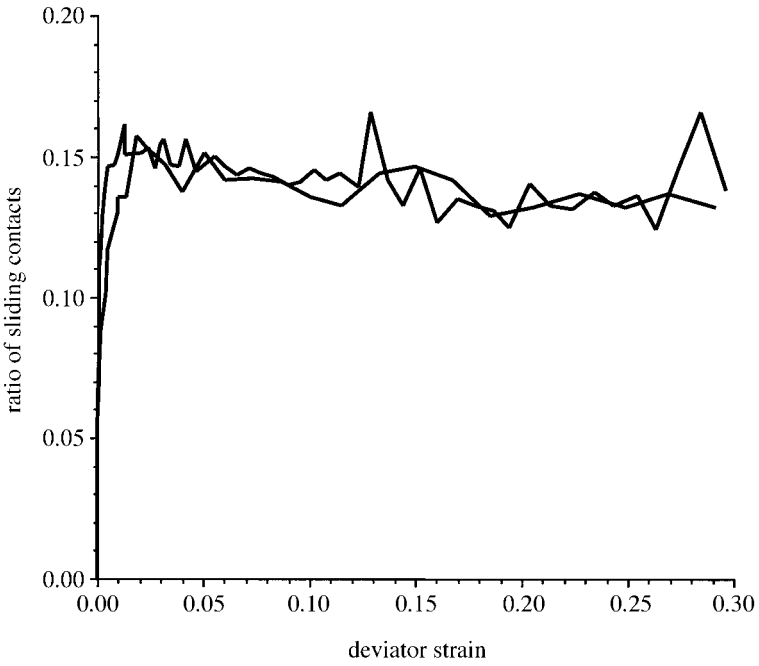

Figure 6. Ratio of sliding contacts.

the mechanical coordination number until a critical value is attained that remains essentially constant thereafter, irrespective of whether the system is expanding or contracting. This critical mechanical coordination number is considered to reflect an underlying physical stability requirement in some way and corresponds, in effect, to a percolation threshold. Figure 6 shows that the ratio of sliding contacts increases to a value that remains essentially constant after about 1% deviator strain and that is independent of the initial packing density.

In real experiments it is difficult to distinguish between the effects of contact friction and particle shape. Numerical simulations allow the effects of contact friction to be isolated. Thornton & Sun (1993) reported simulations of axisymmetric compression using two different coefficients of interparticle friction, $\mu = 0.3$ and $\mu = 0.6$, specified for both the dense and loose systems, with no interparticle adhesion. The results showed that an increase in the interparticle friction resulted in an increase in shear modulus and shear strength for both systems and also resulted in a higher degree of induced structural anisotropy and higher rates of dilation. Although the tangential contact-force contribution to the deviator stress increased with increased interparticle friction, it remained very small in comparison to the normal contact-force contribution, which also increased when the interparticle friction was increased. It was also observed that when the interparticle friction was increased the ratio of sliding contacts decreased and the critical mechanical coordination number decreased.

Further axisymmetric compression test simulations have been performed on the dense system at a constant mean stress of 100 kPa with a different value of μ specified for each test. Figure 7 shows that increasing the interparticle friction reduces the ratio of sliding contacts and, in figure 8, it can be seen that the critical mechanical coordination number decreases if the interparticle friction is increased. All our

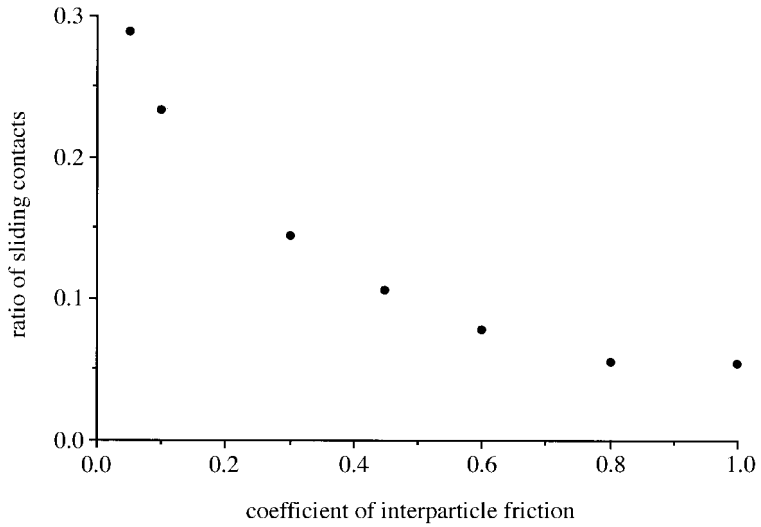

Figure 7. Effect of interparticle friction on the ratio of sliding contacts.

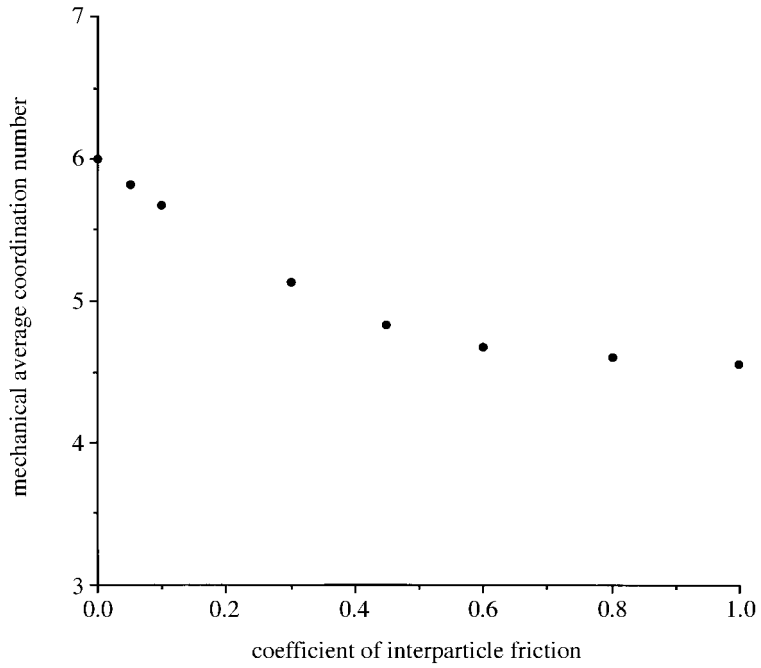

Figure 8. Effect of interparticle friction on the mechanical average coordination number.

simulations have shown that increasing the interparticle friction does not produce a significant increase in the amount of energy dissipated, but decreases the percentage of sliding contacts. This demonstrates that friction acts, primarily, as a kinematic constraint. Enhanced friction at the contacts increases the stability of the system and reduces the number of contacts required to achieve a stable configuration, leading to a reduction in the critical mechanical coordination number. When interparticle sliding

does occur it tends to be at the relatively unloaded contacts in the regions between the chains of particles transmitting large forces (as described in § 4). Consequently, the tangential contact-force contribution to the deviator stress is small.

4. Force transmission

For any assemblage of discrete particles subjected to external loading, the transmission of force from one boundary to another can only occur via the interparticle contacts. Intuitively, therefore, we expect that the distribution of contacts will determine the distribution of forces within the system of particles, and that the forces will not necessarily be distributed uniformly. Direct observations of stress distribution in photoelastic studies of two-dimensional arrays of discs have been reported by Dantu (1957), de Josselin de Jong & Verruijt (1969), Drescher & de Josselin de Jong (1972) and Oda & Konishi (1974). Konishi *et al*. (1982) used the same photoelastic technique to examine arrays of oval-shaped particles. In all photoelastic studies of disc assemblies it has been observed that the load is largely transmitted by relatively rigid, heavily stressed chains of particles forming a relatively sparse network of above-average contact forces. Groups of particles separating the strong force chains are only lightly loaded. The implication is that, in a random system of particles, the applied load will search for the shortest and most direct transmission path, and the straighter the chosen pathway (less of a zig-zag) the higher the proportion of load that will be transmitted.

Cundall & Strack (1979) numerically simulated a simple shear test and demonstrated good qualitative agreement obtained between the simulated force transmission patterns and those obtained in the corresponding photoelastic disc experiment reported by Oda & Konishi (1974). Thornton & Barnes (1986) reported two-dimensional simulations of quasi-static shear deformation of a compact polydisperse system of 1000 discs using the BALL code and provided visualizations of the force transmission patterns obtained under isotropic and anisotropic states of stress. Even when both the microstructure and the stress state were isotropic, some contacts transmitted forces several times those of others but there was no preferred direction for the larger contact forces. Under anisotropic stress conditions, the large forces were orientated in the direction of the major principal stress. It was observed that the contact-force obliquity along high-force chains was low, whereas the ratio of tangential to normal contact forces was much higher in the relatively unloaded regions and sliding tended to occur at contacts that carried small forces.

Using the three-dimensional simulation code TRUBAL, quasi-static deformation tests have been simulated in a periodic cell on polydisperse systems of 8000 elastic spheres. Thornton (1997*b*) provided visualizations to illustrate the contact-force transmission through such a system when subjected to an axisymmetric stress state ($\sigma_1 > \sigma_2 = \sigma_3$). When viewed in the direction of σ_1, large forces were evident but there appeared to be no directional bias, due to the fact that both the structure and the state of stress were isotropic in the plane orthogonal to the viewing direction. However, when the force transmission was viewed in a direction orthogonal to the σ_1 direction, it was clear that the strong forces tended to align themselves in the σ_1 direction. Experimental evidence of strong force chains in three-dimensional packings of spheres has been demonstrated by Liu *et al*. (1995).

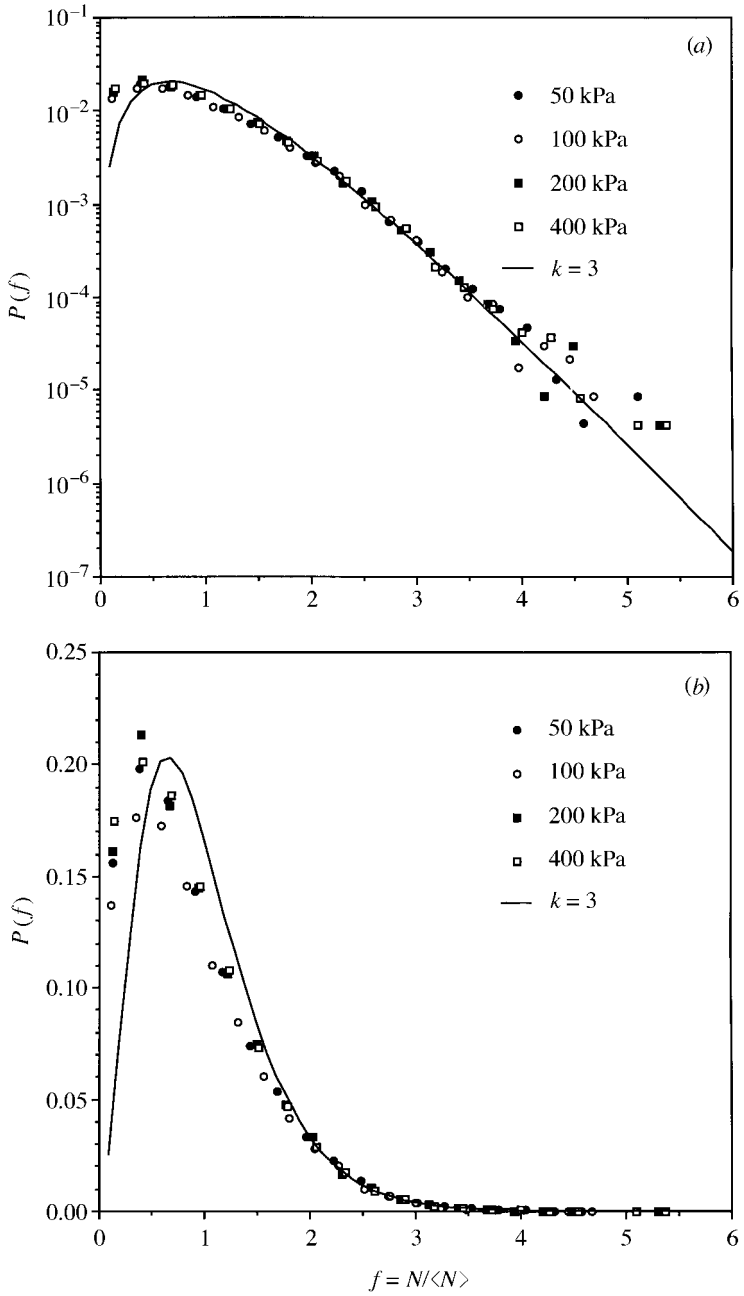

Figure 9. Normal contact-force distribution at isotropic stress states of 50, 100, 200 and 400 kPa (hard-sphere system).

Liu *et al.* (1995) also used a layer of carbon paper on the inside surface of a cylindrical container to examine the distribution of forces on the base when the container was filled with beads. Their results indicated that the number of contacts carrying a given force decreased exponentially as the magnitude of the force increased. A simple

theoretical model was proposed for the probability distribution of the magnitude of the normal contact forces (see also Coppersmith *et al*. 1996). The model assumes that the inhomogeneity of the particle arrangement causes an unequal distribution of force transmission between contiguous particles, which leads to chains of particles transmitting above-average forces. Adopting a stochastic analysis, a mean-field solution for the probability distribution was obtained that may be written in the form

$$P(f) = \frac{k^k}{(k-1)!} f^{k-1} \exp(-kf), \quad \text{where } f = \frac{N}{\langle N \rangle}, \tag{4.1}$$

and $\langle N \rangle$ is the average normal contact force.

We have performed three-dimensional simulations of two polydisperse systems of 8000 elastic spheres subjected to isotropic compression in a periodic cell. The only difference in the particle specifications was that one system was composed of 'hard' spheres and the other of 'soft' spheres. The particles in the hard-sphere system were attributed with a Young's modulus, $E = 70$ GPa; a value of $E = 70$ MPa was specified for the particles in the soft-sphere system. Both systems were isotropically compressed to stress levels of 50, 100, 200 and 400 kPa. Figure 9 shows that the contact-force distributions obtained for the hard-sphere system are insensitive to stress level. Superimposed on the figure, is the theoretical model given by equation (4.1) with $k = 3$. Although the theoretical model reflects the exponential distribution of the large contact forces, it only agrees reasonably well with the data sets for contact forces that are more than twice the magnitude of the average contact force, and fails to capture the distribution of the below-average contact forces.

The contact-force distributions obtained for the soft-particle system (figure 10), clearly show that the distribution of the above-average forces depends on the stress level. The results indicate that as the stress level is increased, the contact force tends towards a Gaussian distribution in which there is a more equal sharing of the load between all of the contacts. The implication is that the same trend would be observed for the hard-particle system if it were subjected to a sufficiently high stress level. Figures 11 and 12 illustrate how the contact-force distribution changes during shear, for the hard and soft-particle systems, respectively. It can be seen that, in both cases, the above-average contact forces tend to follow a more exponential distribution and that there is an increase in the proportion of contacts carrying below-average contact forces.

Radjai *et al*. (1996) examined force networks in numerical simulations of two-dimensional systems of rigid spheres. In a rigid-sphere array, the contact force is not a function of the relative displacement of the two spheres forming the contact, but is the result of the geometrical configuration of the whole system and the boundary conditions. The simulation technique has been termed the contact dynamics method and is described by Moreau (1994). From the probability distributions obtained, Radjai *et al*. (1996) found that although the above-average normal contact forces exhibited an exponential decay, the smaller than average normal contact forces had a power-law distribution. They suggested that the probability, $P(f)$, takes the form

$$P(f) \propto f^{\alpha}, \qquad f < 1, \tag{4.2}$$

$$P(f) \propto \exp[\beta(1-f)], \qquad f > 1. \tag{4.3}$$

From all of our simulations, whether they be of a hard or a soft system under isotropic compression or at any stage during shear, we find that, for contacts trans-

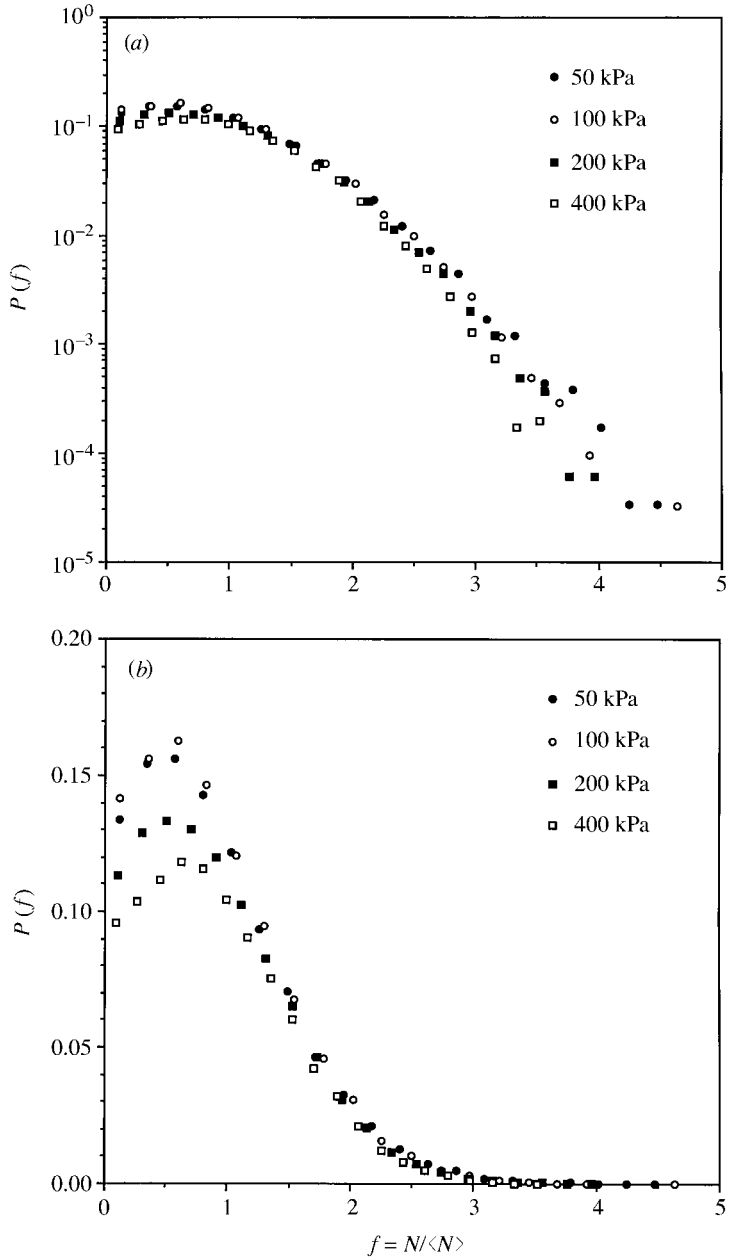

Figure 10. Normal contact-force distribution at isotropic stress states of 50, 100, 200 and 400 kPa (soft-sphere system).

mitting small forces ($f < 0.5$), the distribution follows a power law defined by (4.2) with $\alpha = -0.16$, which may be compared with the value of $\alpha = -0.3$ reported by Radjai *et al*. (1996). Considering the contact-force distributions obtained for the hard-sphere system shown in figure 9, we find that the best fit to the data using (4.3) is obtained with $\beta = 2.15$, compared with the reported value, $\beta = 1.4$, in Radjai *et*

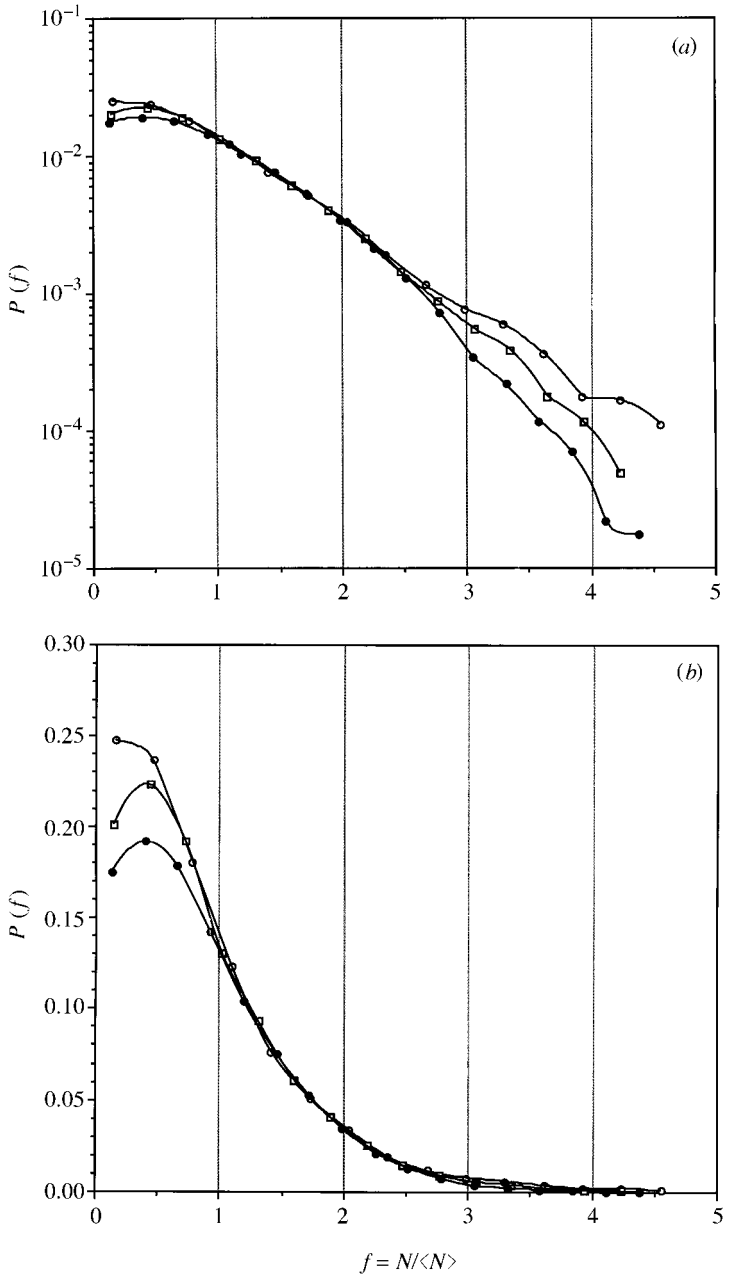

Figure 11. Normal contact-force distribution in the hard-sphere system at the start of shear (•), at maximum deviator stress (○) and at fully developed flow (□).

al. (1996). However, a good fit to the data is only obtained for $f > 2$ and it is clear from figure 10 that (4.3) will not provide a satisfactory representation of the force distribution for soft-particle systems, especially at high stress levels. Furthermore, the inability of (4.2) and (4.3) to fit the data over the range $0.5 < f < 2.0$ is a serious

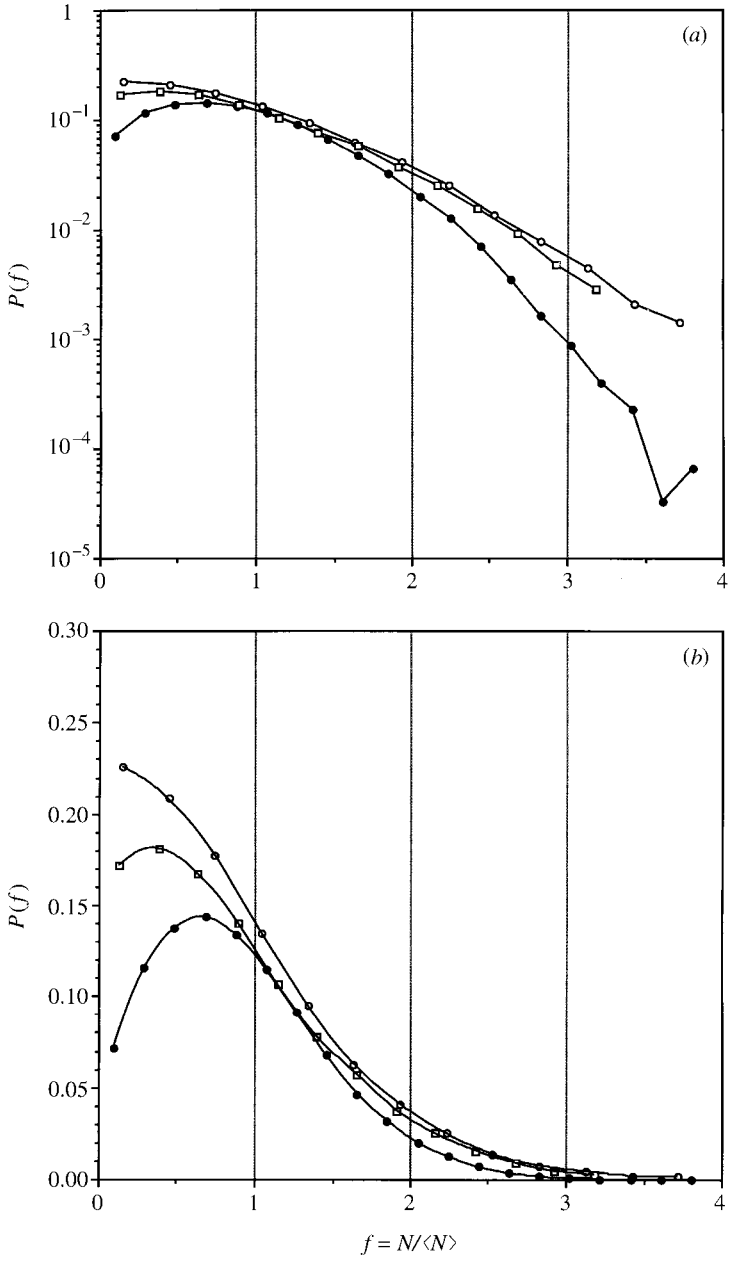

Figure 12. Normal contact-force distribution in the soft-sphere system at the start of shear (•), at maximum deviator stress (○) and at fully developed flow (□).

limitation, since this range accounts for at least half of the contacts. The problem may be resolved by adopting the following empirical function suggested by Mueth *et al.* (1998):

$$P(f) = a[1 - b\exp(-f^2)]\exp(-cf). \tag{4.4}$$

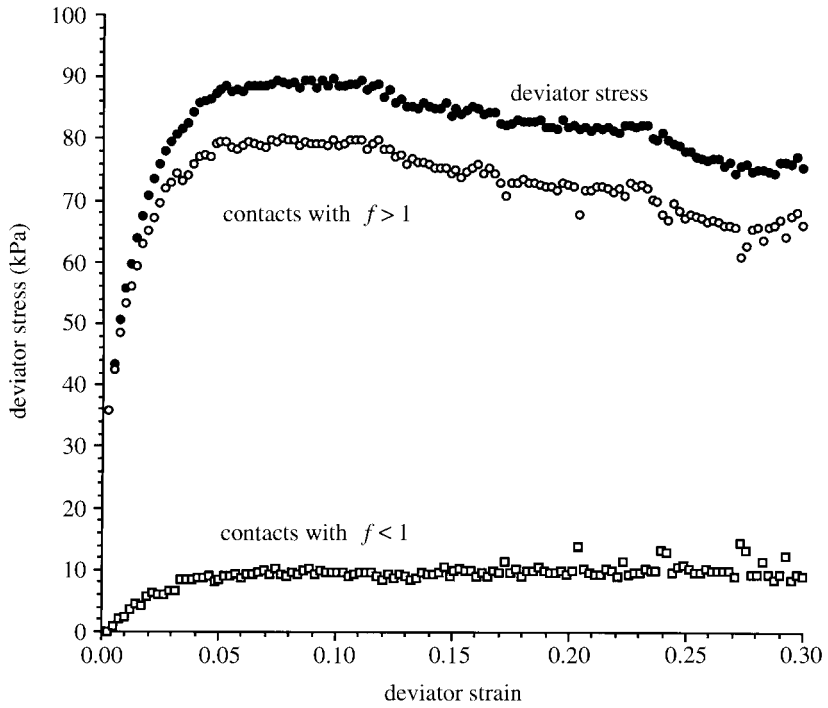

Figure 13. Evolution of the contributions of the weak (□) and strong (○) subnetworks to the deviator stress (●) (hard-sphere system).

5. Strong- and weak-force transmission networks

Radjai *et al*. (1997) suggested that the contact network may be partitioned into two complementary subnetworks: a 'strong' percolating subnetwork of contacts transmitting above-average contact forces; and a 'weak' subnetwork of contacts carrying below-average forces. From two-dimensional simulations of quasi-static biaxial compression on a polydisperse system of *ca.* 4000 rigid discs, they concluded that the strong network accounts for all the deviatoric stress, whereas the weak network contributes only to the mean stress. They also found that the orientation of the induced structural anisotropy in the strong network coincided with the orientation of the stress tensor, as expected, but the orientation of the induced structural anisotropy in the weak network was orthogonal to that of the strong network. In this section we re-examine our own data in terms of strong and weak force-transmission networks and the contribution each makes to both the stress tensor and the fabric tensor.

Figures 13 and 14 illustrate the evolution of the deviator stress and its decomposition into the contributions due to contacts with $f < 1$ and $f > 1$, for the hard and soft systems of 8000 spheres, respectively, when subjected to axisymmetric compression, with the mean stress maintained constant at 100 kPa. The figures clearly show that the contribution of the weak network of contacts is small, never exceeding 13% for the hard-particle system and never deviating from an isotropic stress state by more than ±4 kPa for the system of soft particles. Inspection of the data reveals that 70% of the contacts in the hard-sphere system carry below-average forces and contribute to 40% of the mean stress. In the soft-sphere system, the weak network

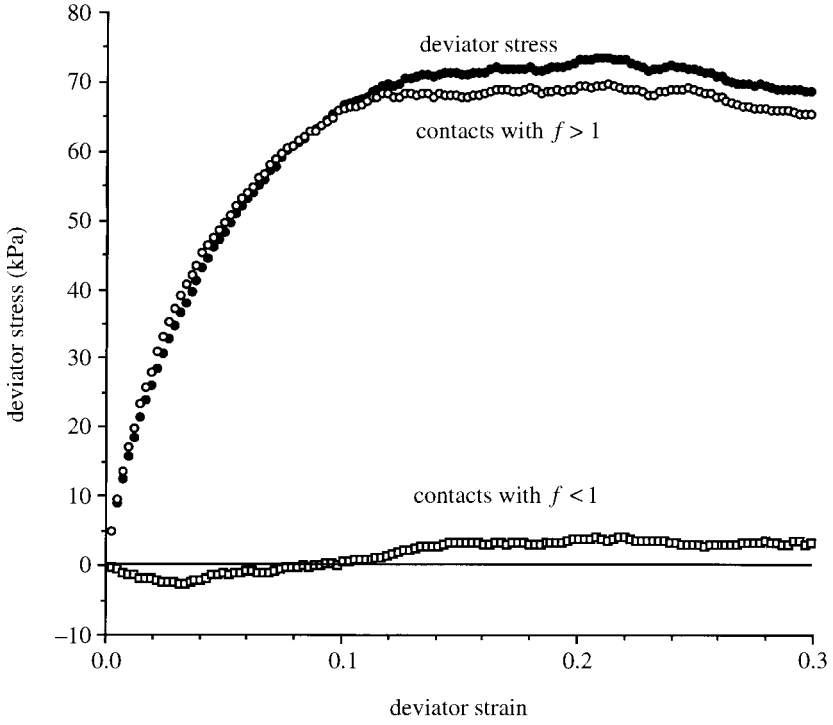

Figure 14. Evolution of the contributions of the weak (□) and strong (○) subnetworks to the deviator stress (●) (soft-sphere system).

is composed of *ca.* 67% of all contacts and their contribution to the mean stress is *ca.* 35%. It is interesting to note that the 5% (3%) of contacts transmitting forces greater than twice the average contact force in the hard (soft) sphere systems only contribute to 40% (45%) of the deviator stress. This emphasizes the need for a probability distribution function, $P(f)$, that fits the data over the complete range $f > 1$.

The evolution of the deviator fabric $(\phi_1 - \phi_3)$ during shear for the two systems is shown in figures 15 and 16. The structural-anisotropy tensor may be partitioned as follows:

$$\phi_{ij} = (1 - q)\phi_{ij}^{\mathrm{W}} + q\phi_{ij}^{\mathrm{S}}, \tag{5.1}$$

where the superscripts 'W' and 'S' indicate the weak and strong subnetworks, and q is the proportion of contacts with $f > 1$. The structural anisotropy tensor has also been calculated for the weak and strong networks separately, and the evolution of the corresponding deviator fabrics are superimposed on the two figures. The subnetwork of contacts with $f > 1$ develops a strongly anisotropic structure in both the hard- and soft-particle systems. The weak subnetworks are only slightly anisotropic and, in agreement with the two-dimensional simulation data for rigid discs obtained by Radjai *et al.* (1997), there are more contacts orientated orthogonal to the major principal stress direction in the case of the soft system. In the hard-particle system, although the orientation of the structural anisotropy of the weak subnetwork is initially orthogonal to the major principal stress direction, after 4% deviator strain the orientation coincides with that of the stress tensor.

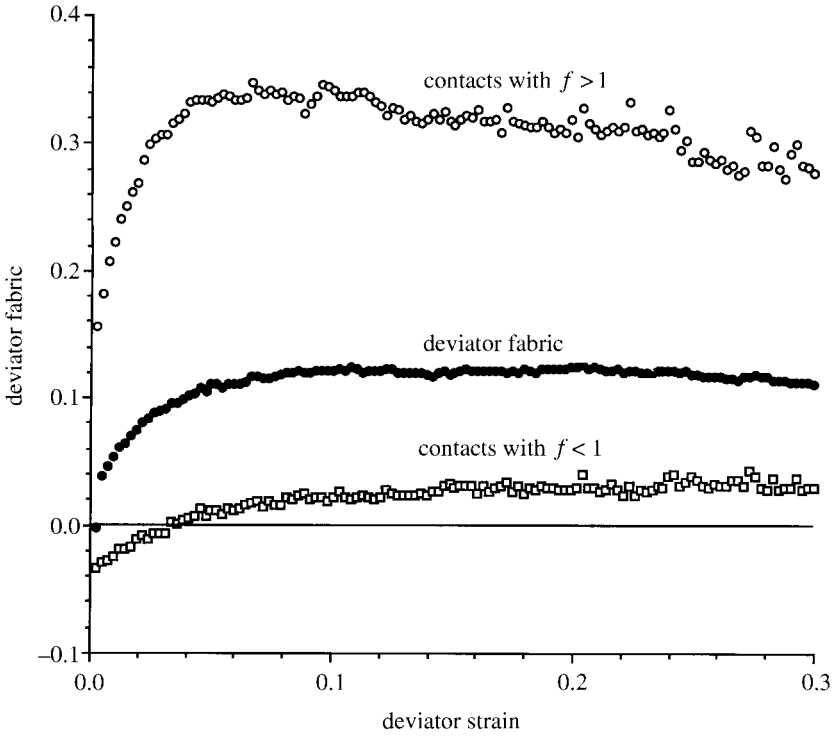

Figure 15. Evolution of the contributions of the weak (□) and strong (○) subnetworks to the induced structural anisotropy (●) (hard-sphere system).

Any conclusions drawn from the data presented in figures 13–16 regarding the complementary nature of the strong and weak subnetworks, must also recognize the statistical limitations of a three-dimensional system of only 8000 particles, which is equivalent to a two-dimensional system of 400 discs. The three-dimensional equivalent of the 4000-disc system of Radjai *et al.* (1997) would require *ca.* 250 000 particles. Consequently, until more information from simulations of much larger three-dimensional systems becomes available, it is not unreasonable to assume that the weak network is structurally isotropic and contributes only to the mean stress.

6. Concluding remarks

Results have been presented of numerical simulations of quasi-static deformation of polydisperse systems of elastic spheres. Both macroscopic and microscopic data have been examined, and explanations have been provided for how the ensemble state of stress relates to the nature of the force transmission between the constituent particles for systems with enduring contacts. The next problem is to examine in detail the associated particle kinematics, in order to obtain a clear physical explanation for the shear-induced dilation which is still lacking. Further work is also required to examine the transition to and from rapid granular flow in which the particle interactions are predominantly collisional. Since numerical simulation provides access to quantitative information about the micromechanical processes occurring at the particle scale, it is the key to obtaining a reliable understanding of the physics of granular media in

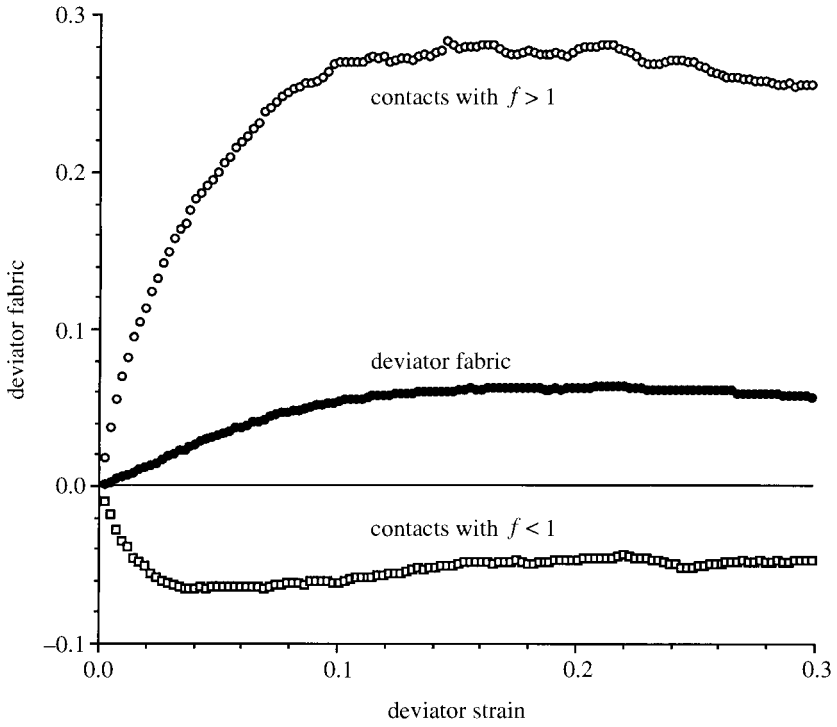

Figure 16. Evolution of the contributions of the weak (□) and strong (○) subnetworks to the induced structural anisotropy (●) (soft-sphere system).

its various states that may lead to physically realistic continuum models necessary to tackle engineering scale problems.

The numerical simulations were carried out during projects supported by the Engineering and Physical Sciences Research Council (grant nos GR/H14427 and GR/K05832). C.T. thanks S. Edwards, A. Liu, S. Nagel, R. Ball, S. Alexander and especially T. Witten for stimulating discussions on force transmission in granular media at the Institute of Theoretical Physics, University of California at Santa Barbara during August 1997, and is grateful for the financial contribution provided through National Science Foundation grant no. PHY94-07194.

References

Barnes, D. J. 1985 A study of the micro-mechanics of granular material. PhD thesis, Aston University, UK.

Coppersmith, S. N., Liu, C.-H., Majumdar, S., Narayan, O. & Witten, T. A. 1996 Model for force fluctuations in bead packs. *Phys. Rev.* E **53**, 4673–4685.

Cundall, P. A. 1988 Computer simulations of dense sphere assemblies. In *Micromechanics of granular materials* (ed. M. Satake & J. T. Jenkins), pp. 113–123. Amsterdam: Elsevier.

Cundall, P. A. & Strack, O. D. L. 1979 A discrete numerical model for granular assemblies. *Géotechnique* **29**, 47–65.

Cundall, P. A. & Strack, O. D. L. 1983 Modeling of microscopic mechanisms in granular materials. In *Mechanics of granular materials: new models and constitutive relationships* (ed. J. T. Jenkins & M. Satake), pp. 137–149. Amsterdam: Elsevier.

Dantu, P. 1957 A contribution to the mechanical and geometrical study of non-cohesive masses. In *Proc. 4th Int. Conf. on Soil Mechanics & Foundation Engineering*, pp. 144–148. London: Butterworths.

de Josselin de Jong, G. & Verruijt, A. 1969 Étude photo-élastique d'un empilement de disques. *Cahiers du Groupe Francais de Rheologie* **2**, 73–86.

Drescher, A. & de Josselin de Jong, G. 1972 Photoelastic verification of a mechanical model for the flow of a granular material. *J. Mech. Phys. Solids* **20**, 337–351.

Konishi, J., Oda, M. & Nemat-Nasser, S. 1982 Inherent anisotropy and shear strength of assembly of oval cross-sectional rods. In *Deformation and failure of granular materials* (ed. P. A. Vermeer & H. J. Luger), pp. 403–412. Rotterdam: Balkema.

Liu, C.-H., Nagel, S. R., Schecter, D. A., Coppersmith, S. N., Majumdar, S., Narayan, O. & Witten, T. A. 1995 Force fluctuations in bead packs. *Science* **269**, 513–515.

Moreau, J.-J. 1994 Some numerical methods in multibody dynamics: applications to granular materials. *Euro. J. Mech.* A **13**, 93–114.

Mueth, D. M., Jaeger, H. M. & Nagel, S. R. 1998 Force distribution in a granular medium. *Phys. Rev.* E **57**, 3164–3169.

Oda, M. & Konishi, J. 1974 Microscopic deformation mechanism of granular material in simple shear. *Soils Foundations* **14**, 25–38.

Radjai, F., Jean, M., Moreau, J.-J. & Roux, S. 1996 Force distributions in dense two-dimensional granular systems. *Phys. Rev. Lett.* **77**, 274–277.

Radjai, F., Wolf, D. E., Roux, S., Jean, M. & Moreau, J.-J. 1997 Force networks in dense granular media. In *Powders and grains* (ed. R. P. Behringer & J. T. Jenkins), vol. 97, pp. 211–214. Rotterdam: Balkema.

Satake, M. 1982 Fabric tensor in granular materials. In *Deformation and failure of granular materials* (ed. P. A. Vermeer & H. J. Luger), pp. 63–68. Rotterdam: Balkema.

Thornton, C. 1997*a* Coefficient of restitution for collinear collisions of elastic-perfectly plastic spheres. *J. Appl. Mech.* **64**, 383–386.

Thornton, C. 1997*b* Force transmission in granular media. *KONA Powder and Particle* **15**, 81–90.

Thornton, C. & Barnes, D. J. 1986 Computer simulated deformation of compact granular assemblies. *Acta. Mechanica* **64**, 45–61.

Thornton, C. & Sun, G. 1993 Axisymmetric compression of three-dimensional polydisperse systems of spheres. In *Powders and grains* (ed. C. Thornton), vol. 93, pp. 129–134. Rotterdam: Balkema.

Thornton, C. & Sun, G. 1994 Numerical simulation of general three-dimensional quasi-static shear deformation of particulate media. In *Numerical methods in geotechnical engineering* (ed. I. M. Smith), pp. 143–148. Rotterdam: Balkema.

Thornton, C. & Yin, K. K. 1991 Impact of elastic spheres with and without adhesion. *Powder Technol.* **65**, 153–166.